Numerical models and stability analysis of control-based methods for nonlinear vibration testing

G. Raze, T. Zhou
University of Liège, Aerospace and Mechanical Engineering Department,
Allée de la Découverte 9, 4000 Liège, Belgium
e-mail: **g.raze@uliege.be**

Abstract

Control-based methods have been proposed over the last two decades as robust means to perform nonlinear vibration testing. These approaches leverage feedback control to stabilize all equilibria and require limited information about the system under test to be effective. However, their control parameters are often tuned through trial and error and systematic tuning methods are lacking in the literature. The purpose of this work is to build accurate numerical models of these control-based methods to evaluate their performance and stability. Such models can clearly indicate the stability boundaries of different equilibria, and can provide valuable insight into potential destabilizing mechanisms. Governing differential equations are derived for CBC and PLL closed-loop systems. They are then solved with the harmonic balance method, and a stability analysis based on Hill's method is also developed. The models are assessed with a Duffing oscillator, and the discrepancies between different filtering and control-based methods are highlighted.

1 Introduction

With the advent of highly flexible structures made up of advanced materials and complex interfaces, the occurrence of nonlinear vibrations is increasingly encountered during vibration testing campaigns. Even though experimental modal analysis is a mature tool that is extensively used in academia and industry [1], its basic assumptions make it fundamentally inapplicable to nonlinear systems. This has motivated the development of a variety of nonlinear system identification techniques to cope with the unique features exhibited by nonlinear dynamical systems [2].

Control-based methods have been proposed as robust testing approaches to overcome the difficulties associated with nonlinear systems testing. The pioneering work of Sieber and Krauskopf [3] introduced the control-based continuation (CBC) method, which consists in using a feedback proportional-integral-derivative (PID) controller in the test to stabilize the unstable responses of a structure. The nonlinear frequency response (NFR) of this structure can then be traced out using algorithms for numerical continuation. Barton et al [4] later proposed a simplification of the continuation approach. Alternatively, the introduction of a phase-locked loop (PLL) was proposed by Peter and Leine [5], wherein a feedback controller is used to automatically adjust the excitation frequency to a desired phase lag between the forcing and the response. This controller also has a stabilizing effect, allowing for the measurement of complete NFRs [6]. Recently, the response-controlled stepped-sine testing (RCT) method was also proposed, featuring the same appealing advantages [7].

In most cases, the different parameters of the system are tuned on a trial-and-error basis. A complete exploration of the parameter space is possible [8] but is generally time consuming. There is only a handful of theoretical works addressing the effect of the parameters on stability of a single-degree-of-freedom Duffing oscillator [6, 9, 10]. Adaptive controllers were also recently proposed and theoretically studied [11, 12], but they have stringent requirements for an experimental implementation (such as full-state feedback). Therefore, practitioners must currently rely on their intuition and trial and error to find suitable parameters.

This work aims to address this issue by developing accurate numerical models for control-based experiments

and their periodic equilibria. Section 2 introduces the three main elements of a setup tested with a control-based method, namely the structure under test, a signal analyzer, and a controller. Section 3 develops the equations of motion of a structure under test, and Section 4 discusses the dynamics of filters required to analyze the structural outputs. Section 5 presents the two most popular control-based methods, namely CBC and PLL, and derives first-order ordinary differential equations (ODEs) for their controller. Section 6 then assembles the derived ODEs with the structural dynamics equations and develops a harmonic balance (HB) formalism to find the periodic solutions of these ODEs as well as their stability. Section 7 demonstrates the proposed HB models with a Duffing oscillator. The results are verified against time simulations, and the stability boundaries are delineated in the parameters space. The conclusions and perspectives of this work are finally drawn in Section 8.

2 Control-based methods

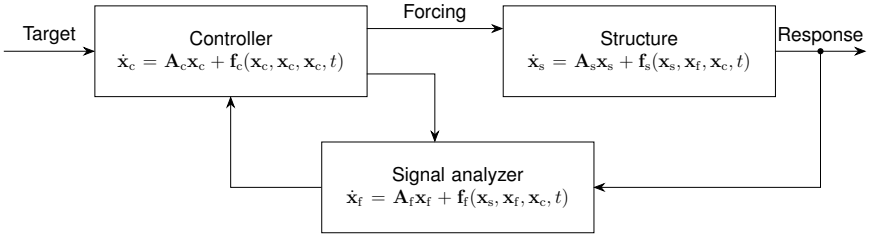

Figure 1: Schematics of a general control-based experiment.

A typical setup using a control-based method consists of three main elements depicted in Figure 1: a structure under test, a signal analyzer (which is typically a filter), and a controller. The structure is excited by the controller, and its output is processed by the signal analyzer. The latter then drives the controller, together with a reference signal y_*. The controller adjusts the input to the structure so as to stir the analyzed structural output toward its desired reference, and (hopefully) also stabilizes this target.

The purpose of the present work is to develop models for the system shown in Figure 1 for two particular control-based methods, namely CBC and PLL. In Sections 3-5, models for these individual elements are developed, and they are assembled in Section 6 to represent the controlled system.

3 Nonlinear structural dynamics

The dynamics of a structure characterized by the vector of generalized degrees of freedom $\mathbf{q}$ can be described by the traditional set of coupled nonlinear second-order ODEs

$$\mathbf{M}\ddot{\mathbf{q}}(t) + \mathbf{C}\dot{\mathbf{q}}(t) + \mathbf{K}\mathbf{q}(t) + \mathbf{p}_\mathrm{nl}(\mathbf{q}(t), \dot{\mathbf{q}}(t), t) = \mathbf{p}_\mathrm{ext}(t) + \mathbf{p}_\mathrm{c}(t), \tag{1}$$

where $\mathbf{M}$, $\mathbf{C}$ and $\mathbf{K}$ are linear structural mass, damping and stiffness matrices, respectively, $\mathbf{p}_\mathrm{nl}$ is the vector of nonlinear and parametric forces, $\mathbf{p}_\mathrm{ext}$ is the vector of external forces and $\mathbf{p}_\mathrm{c}$ is the vector of control forces. For the sake of simplicity, these equations can be recast into a set of first-order ODEs (provided the mass matrix is invertible) using the state vector $\mathbf{x}_\mathrm{s}^T = \begin{bmatrix}\mathbf{q}^T & \dot{\mathbf{q}}^T\end{bmatrix}$ and

$$\dot{\mathbf{x}}_\mathrm{s}(t) = \begin{bmatrix}\dot{\mathbf{q}}(t) \\ \ddot{\mathbf{q}}(t)\end{bmatrix} = \begin{bmatrix}\mathbf{0} & \mathbf{I} \\ -\mathbf{M}^{-1}\mathbf{K} & -\mathbf{M}^{-1}\mathbf{C}\end{bmatrix}\begin{bmatrix}\mathbf{q}(t) \\ \dot{\mathbf{q}}(t)\end{bmatrix} + \begin{bmatrix}\mathbf{0} \\ \mathbf{M}^{-1}\left(\mathbf{p}_\mathrm{ext}(t) + \mathbf{p}_\mathrm{c}(t) - \mathbf{p}_\mathrm{nl}(\mathbf{q}(t), \dot{\mathbf{q}}(t), t)\right)\end{bmatrix}, \tag{2}$$

where $\mathbf{I}$ is the identity matrix. Equation (2) can also be rewritten in the compact form

$$\dot{\mathbf{x}}_\mathrm{s}(t) = \mathbf{A}_\mathrm{s}\mathbf{x}_\mathrm{s}(t) + \mathbf{f}_\mathrm{nl,s}(\mathbf{x}_\mathrm{s}(t), t) + \mathbf{f}_\mathrm{ext,s}(t) + \mathbf{f}_\mathrm{s,c}(t), \tag{3}$$

separating explicitly the linear, nonlinear, external and control forces.

The output signal and its time derivative (typically corresponding to a displacement and an associated velocity) are assumed to be obtainable from the state vector with the matrices $\mathbf{C}_\mathrm{q}$ and $\mathbf{C}_{\dot{\mathrm{q}}}$, respectively, as

$$x(t) = \mathbf{C}_\mathrm{q}\mathbf{x}_\mathrm{s}(t), \qquad \dot{x}(t) = \mathbf{C}_{\dot{\mathrm{q}}}\mathbf{x}_\mathrm{s}(t). \tag{4}$$

4 Filter dynamics

Representative quantities of periodic structural responses for control-based methods can be obtained from a Fourier decomposition of the signal x, which can itself be performed by an adequate filter. The goal of the filter is thus to provide an estimate of a truncated Fourier decomposition

$$x(t) = \mathbf{Q}(\theta(t))\mathbf{w}(t), \tag{5}$$

where $\mathbf{w}$ is a column vector containing the estimates of the Fourier coefficients, $\mathbf{Q}(t)$ is a row vector of h harmonic functions

$$\mathbf{Q}(\theta(t)) = \left[\frac{1}{\sqrt{2}} \quad \sin(\theta(t)) \quad \cos(\theta(t)) \quad \sin(2\theta(t)) \quad \cos(2\theta(t)) \quad \cdots \quad \sin(h\theta(t)) \quad \cos(h\theta(t))\right], \tag{6}$$

and $\theta(t)$ represents the instantaneous fundamental phase of these harmonic functions.

4.1 Perfect filter

Ideally, for a periodic solution and a perfect Fourier decomposition, the coefficients $\mathbf{w}$ are constant and satisfy

$$\mathbf{w} = \frac{\omega}{\pi}\int_0^{2\pi/\omega} \mathbf{Q}^T(\omega t)x(t)dt. \tag{7}$$

However, the filters used in practice are not perfect. Hence, a time dependence on the coefficients $\mathbf{w}$ is retained to reflect the associated filter dynamics.

4.2 Synchronous demodulation

A popular approach to extract the harmonic components of a signal is synchronous demodulation. In this approach, the signal is multiplied by harmonic functions and low-pass filtered. With a first-order, unit-gain low-pass filter, this process reads

$$\dot{\mathbf{w}}(t) = -\omega_\mathrm{lp}\mathbf{w}(t) + 2\omega_\mathrm{lp}x(t)\mathbf{Q}^T(\theta(t)), \tag{8}$$

where ω_lp is the cut-off frequency of the filter.

4.3 Adaptive filter

Adaptive filters constitute an alternative to synchronous demodulation. They are widely used as effective noise cancellation means [13] and were leveraged in [14] to perform online Fourier decomposition. Different adaptation laws exist to set the Fourier coefficients $\mathbf{w}$ as a function of the input signal x. In this work, the Widrow-Hoff least mean squares (LMS) algorithm is used. A continuous-time version of this scheme is [13, 15]

$$\dot{\mathbf{w}}(t) = \mu\left(x(t) - \mathbf{Q}(\theta(t))\mathbf{w}(t)\right)\mathbf{Q}^T(\theta(t)), \tag{9}$$

where μ is the filter gain.

4.4 General filter model

Both Equations (8) and (9) can be put in the general form

$$\dot{\mathbf{x}}_{\mathrm{f}}(t) = \mathbf{A}_{\mathrm{f}}\mathbf{x}_{\mathrm{f}}(t) + \mathbf{f}_{\mathrm{f}}(\mathbf{x}_{\mathrm{s}}(t), \mathbf{x}_{\mathrm{f}}(t), \mathbf{x}_{\mathrm{c}}(t), t), \tag{10}$$

where $\mathbf{x}_{\mathrm{f}}$ is the state vector associated with the filter(s) and generally contains the Fourier coefficients of one (or multiple) signal(s), and $\mathbf{x}_{\mathrm{c}}$ is the state vector of the controller (that will be explicited in Section 5). The dependency of $\mathbf{f}_{\mathrm{f}}$ on $\mathbf{x}_{\mathrm{s}}$ and $\mathbf{x}_{\mathrm{c}}$ is due to x and $\theta(t)$, respectively.

5 Models for control-based methods

The two most popular variants of control-based methods, namely CBC and PLL, are presented hereafter. Their dynamics is also described through ODEs.

5.1 Control-based continuation

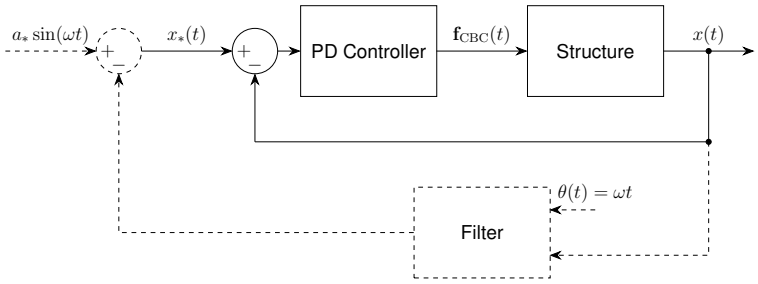

Figure 2: Schematics of the CBC method.

A general implementation of the CBC method is schematized in Figure 2. A PD controller is used to stabilize (if possible) all solutions within the test range by stirring the measured output of the system, x, toward a desired reference x_*. The PD controller outputs a force which reads

$$\mathbf{f}_{\mathrm{CBC}}(t) = \mathbf{B}\left(k_{\mathrm{p}}\left(x_*(t) - x(t)\right) + k_{\mathrm{d}}\left(\dot{x}_*(t) - \dot{x}(t)\right)\right), \tag{11}$$

where $\mathbf{B}$ is an influence vector describing the spatial distribution of the force. To this is adjoined the non-invasiveness condition

$$k_{\mathrm{p}}(x_*(t) - x(t)) + k_{\mathrm{d}}(\dot{x}_*(t) - \dot{x}(t)) = f(t), \tag{12}$$

which requires that the forcing defined by Equation (11) is equal to a desired force profile f. This subjects the structure to open-loop excitation conditions, which is a sufficient condition to ensure that the equilibria of the closed-loop system will be identical to those of the open-loop system. The stability of these equilibria will nevertheless be altered by the action of the PD controller, providing the opportunity to experiment with normally unstable equilibria. In most cases, f is a sinusoidal forcing, and an equivalent requirement to Equation (12) is that $x_* - x$ be tonal.

In practice, the signal x_* is adapted to guarantee the non-invasiveness condition. This can be performed in three ways:

1. Using a Newton-Raphson method that adapts the Fourier coefficients of x_* to satisfy Equation (12) [3].
2. Using a Picard iteration scheme that sets the non-fundamental Fourier coefficients of x_* equal to those of x [4].
3. Using an adaptive filter that automatically sets the signal x_* [9, 14], as schematically depicted in the dashed part of Figure 2.

As opposed to the two first possibilities, the third one can be modeled by a continuous-time process. For the latter, the dynamic effect of the filter can be included. For the two first ways, the models developed herein can only deal with the dynamics of the closed-loop systems once the iterative schemes have converged to a non-invasive solution, but cannot assess the convergence of these schemes themselves.

Using a filter, non-invasiveness can be achieved if

$$x_*(t) = a_* \sin(\omega t) + b_* \cos(\omega t) + \mathbf{Q}(\theta(t))\mathbf{P}_{\mathrm{nf}}\mathbf{w}(t), \tag{13}$$

where a_* and b_* can either be adapted to satisfy Equation (12) or given arbitrary values, and $\mathbf{P}_{\mathrm{nf}}$ is a matrix selecting the non-fundamental harmonic coefficients (cf. Equations (5) and (6))

$$\mathbf{P}_{\mathrm{nf}} = \mathbf{I} - \left(\mathbf{e}_2\mathbf{e}_2^T + \mathbf{e}_3\mathbf{e}_3^T\right), \tag{14}$$

with $\mathbf{e}_i$ the i^{th} canonical basis vector of $\mathbb{R}^{2h+1}$. In this way, x_* has the same non-fundamental harmonics as x, making their difference a purely sinusoidal signal.

5.2 Phase-locked loop

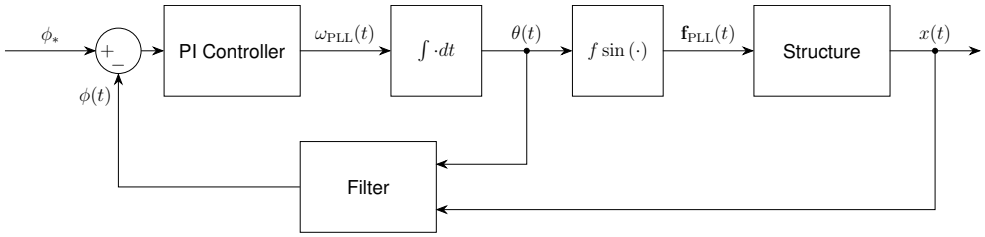

Figure 3: Schematics of the PLL method.

The block diagram representing a structure controlled with a PLL is schematized in Figure 3. In this system, the frequency of excitation ω_{PLL} is automatically adjusted by a PI controller to enforce the phase of the fundamental harmonic of the response ϕ to equate a desired reference phase ϕ_*. The frequency of excitation is given by the output of a PI controller by

$$\omega_{\mathrm{PLL}}(t) = \omega(0) + k_{\mathrm{i}} \int_0^t \left(\phi(\tau) - \phi_*\right) d\tau + k_{\mathrm{p}} \left(\phi(\mathbf{w}(t)) - \phi_*\right), \tag{15}$$

where ϕ is the phase lag of the response that can be estimated by

$$\phi(\mathbf{w}(t)) = \arctan\left(\frac{w_{\mathrm{c},1}}{w_{\mathrm{s},1}}\right), \tag{16}$$

$w_{\mathrm{s},1}$ and $w_{\mathrm{c},1}$ being the fundamental sine and cosine coefficients, respectively, of the Fourier decomposition (Equation (5)). The forcing imposed by the PLL to the structure is then

$$\mathbf{f}_{\mathrm{PLL}}(t) = \mathbf{B} f \sin\left(\int_0^t \omega_{\mathrm{PLL}}(\tau) d\tau\right). \tag{17}$$

Equations (15) and (17) are integro-differential equations that can be manipulated to obtain ODEs with periodic quantities treatable by a HB formalism (if periodic solutions of the controlled systems are sought). First, since the frequency is the output of a (linear) PI controller, it is decomposed into

$$\omega_{\mathrm{PLL}}(t) = \omega + \omega_{\mathrm{i}}(t) + \omega_{\mathrm{p}}(t), \tag{18}$$

where ω is the average value of $\omega_{\mathrm{PLL}}(t)$ (for periodic solutions), and $\omega_{\mathrm{p}}(t)$ and $\omega_{\mathrm{i}}(t)$ are fluctuations due to the proportional and integral terms (that will be formally defined by Equations (21) and (22)), respectively.

As a consequence, the instantaneous phase θ is given by

$$\theta(t) = \int_0^t \omega_{\mathrm{PLL}}(\tau)d\tau = \omega t + \int_0^t \left(\omega_{\mathrm{i}}(\tau) + \omega_{\mathrm{p}}(\tau)\right) d\tau = \omega t + \theta_{\mathrm{pi}}(t), \tag{19}$$

where θ_{pi} represents a periodic phase fluctuation due to the PI controller. Inserting Equation (19) into Equation (17), the PLL forcing thus becomes

$$\mathbf{f}_{\mathrm{PLL}}(t) = \mathbf{B} f \sin(\omega t + \theta_{\mathrm{pi}}(t)), \tag{20}$$

where θ_{pi} is governed by the ODE

$$\dot{\theta}_{\mathrm{pi}}(t) = \omega_{\mathrm{i}}(t) + \omega_{\mathrm{p}}(t) = \omega_{\mathrm{i}}(t) + k_{\mathrm{p}} \left(\phi(\mathbf{w}(t)) - \phi_*\right), \tag{21}$$

and ω_{i} by

$$\dot{\omega}_{\mathrm{i}}(t) = k_{\mathrm{i}} \left(\phi(\mathbf{w}(t)) - \phi_*\right). \tag{22}$$

Equations (20)-(22) are equivalent to Equations (15) and (17), but are ODEs that only feature time-periodic quantities when time-periodic solutions are sought.

5.3 General model

For the PLL, gathering θ and ω_{i} into a state vector $\mathbf{x}_{\mathrm{c}}$, Equations (21) and (22) can be put in the general form

$$\dot{\mathbf{x}}_{\mathrm{c}}(t) = \mathbf{A}_{\mathrm{c}}\mathbf{x}_{\mathrm{c}}(t) + \mathbf{f}_{\mathrm{c}}(\mathbf{x}_{\mathrm{s}}(t), \mathbf{x}_{\mathrm{f}}(t), \mathbf{x}_{\mathrm{c}}(t), y_*(t), t), \tag{23}$$

where y_* can be the reference signal x_* for CBC, and the reference phase lag ϕ_* for PLL.

The CBC does not feature direct dynamics (in the sense that it is not governed by an ODE) due to the assumptions made in this work, but influence those of the coupled system through the control force $\mathbf{f}_{\mathrm{s,c}}(t)$. Hence, for the CBC, the state vector $\mathbf{x}_{\mathrm{c}}$ is simply empty.

6 Controlled system dynamics and stability

Having described the dynamics of the individual subsystems of a control-based experiment, it is now possible to assemble them to describe the controlled system dynamics. This provides a set of nonlinear coupled ODEs, that can be solved with the HB formalism. In addition, using Hill's method, the stability of the found solutions can be assessed.

6.1 Controlled system dynamics

The subsystems can be coupled by expressing the control force exerted on the structure as the general expression

$$\mathbf{f}_{\mathrm{s,c}}(t) = \mathbf{B} f_{\mathrm{s,c}}(\mathbf{x}_{\mathrm{s}}(t), \mathbf{x}_{\mathrm{f}}(t), \mathbf{x}_{\mathrm{c}}(t), t, y_*(t)), \tag{24}$$

whose specializations to CBC and PLL are given in Equations (11) and (20), respectively. Eventually, assembling Equations (3), (10), (23) and (24), the coupled system is governed by the first-order ODE

$$\begin{bmatrix} \dot{\mathbf{x}}_{\mathrm{s}}(t) \\ \dot{\mathbf{x}}_{\mathrm{f}}(t) \\ \dot{\mathbf{x}}_{\mathrm{c}}(t) \end{bmatrix} = \begin{bmatrix} \mathbf{A}_{\mathrm{s}} & \mathbf{0} & \mathbf{0} \\ \mathbf{0} & \mathbf{A}_{\mathrm{f}} & \mathbf{0} \\ \mathbf{0} & \mathbf{0} & \mathbf{A}_{\mathrm{c}} \end{bmatrix} \begin{bmatrix} \mathbf{x}_{\mathrm{s}}(t) \\ \mathbf{x}_{\mathrm{f}}(t) \\ \mathbf{x}_{\mathrm{c}}(t) \end{bmatrix} + \begin{bmatrix} \mathbf{f}_{\mathrm{nl,s}}(\mathbf{x}_{\mathrm{s}}(t), t) + \mathbf{B} f_{\mathrm{s,c}}(\mathbf{x}_{\mathrm{s}}(t), \mathbf{x}_{\mathrm{f}}(t), \mathbf{x}_{\mathrm{c}}(t), t, y_*(t)) \\ \mathbf{f}_{\mathrm{f}}(\mathbf{x}_{\mathrm{s}}(t), \mathbf{x}_{\mathrm{f}}(t), \mathbf{x}_{\mathrm{c}}(t), t) \\ \mathbf{f}_{\mathrm{c}}(\mathbf{x}_{\mathrm{s}}(t), \mathbf{x}_{\mathrm{f}}(t), \mathbf{x}_{\mathrm{c}}(t), y_*(t), t) \end{bmatrix} + \begin{bmatrix} \mathbf{f}_{\mathrm{ext,s}}(t) \\ \mathbf{0} \\ \mathbf{0} \end{bmatrix}, \tag{25}$$

which is put in the compact form

$$\dot{\mathbf{x}}(t) = \mathbf{A}\mathbf{x}(t) + \mathbf{f}(\mathbf{x}(t), y_*(t), t) + \mathbf{f}_{\mathrm{ext}}(t), \tag{26}$$

where $\mathbf{x}^T = \begin{bmatrix}\mathbf{x}_\mathrm{s}^T & \mathbf{x}_\mathrm{f}^T & \mathbf{x}_\mathrm{c}^T\end{bmatrix}$ is the state vector of size N_x of the coupled system.

6.2 Harmonic balance formalism

The periodic solutions of Equation (26) are now sought. To compute them, the HB method is used. Following the approach outlined in [16], the state vector is described by means of a truncated Fourier expansion

$$\mathbf{x}(t) = (\mathbf{Q}(\omega t) \otimes \mathbf{I})\,\mathbf{z}, \tag{27}$$

where $\mathbf{z}$ is a vector of size $N_\mathrm{z} = (2N_h + 1)N_\mathrm{x}$ gathering the Fourier coefficients associated with every entry of the state vector, with N_h the number of harmonics used by the method. The operator $\otimes$ represents a Kronecker product. Inserting this ansatz into Equation (26) and using a Galerkin procedure, the frequency-domain counterpart of Equation (26) is obtained as

$$(\mathbf{I} \otimes \mathbf{A} - \nabla(\omega) \otimes \mathbf{I})\,\mathbf{z} + \mathbf{b}(\mathbf{z}, \omega, \xi_*) + \mathbf{b}_\mathrm{ext} = \mathbf{0}, \tag{28}$$

where $\mathbf{b}$ and $\mathbf{b}_\mathrm{ext}$ are the Fourier transforms of $\mathbf{f}$ and $\mathbf{f}_\mathrm{ext}$, respectively, ξ_* is a parameter characterizing $y_*(t)$ (e.g., a_* for CBC and ϕ_* for PLL), and ∇ is a differential operator given by

$$\nabla(\omega) = \begin{bmatrix} 0 & & \mathbf{0} \\ & \begin{bmatrix} 1 & 0 & \cdots & 0 \\ 0 & 2 & \cdots & 0 \\ \vdots & \vdots & \ddots & \vdots \\ 0 & 0 & \cdots & h \end{bmatrix} \otimes \begin{bmatrix} 0 & -\omega \\ \omega & 0 \end{bmatrix} \\ \mathbf{0} & \end{bmatrix}. \tag{29}$$

Equation (28) represents a set of nonlinear algebraic equations that can be solved with standard computer methods. More details on the derivation can be found in [16].

6.3 Continuation

Equation (28) represents a system of N_z equations for $N_z + 2$ variables ($\mathbf{z}$, ω and ξ_*). To be usable with a continuation approach, either one of these variables has to be fixed, or an additional equation is required.

For CBC, the method of Barton et al. [4] is simulated in this work. ω is thus fixed, $b_* = 0$ and $\xi_* = a_*$ is used as a bifurcation parameter. When the filter dynamics are neglected, the vector $\mathbf{x}_\mathrm{f}$ is empty, but the non-fundamental harmonic coefficients of the reference signal x_* are added as unknowns, and the requirement that $x - x_* = a_* \sin(\omega t)$ is added for closure.

For PLL, a phase condition is required since the system is autonomous. Without loss of generality, $\theta_\mathrm{pi}(0) = 0$ is chosen. This adds an equation to the system, making the difference between the number of variables and the number of equation equal to one, i.e., a well-posed problem for continuation. When the filter dynamics are neglected, the vector $\mathbf{x}_\mathrm{f}$ is empty, and the phase ϕ is computed directly from the harmonic coefficients $\mathbf{z}$ (instead of $\mathbf{w}$).

6.4 Stability analysis

If a periodic solution $\mathbf{x}_\mathrm{eq}(t)$ of Equation (26) has be found, it is important to know whether this solution will be stable. In this work, the asymptotic stability of a solution is assessed through a linearization procedure. A small perturbation term $\mathbf{s}$ is added to the equilibrium solution as

$$\mathbf{x}(t) = \mathbf{x}_\mathrm{eq}(t) + \mathbf{s}(t) \tag{30}$$

with $|\mathbf{s}(t)| \ll |\mathbf{x}_{\mathrm{eq}}(t)|$. This perturbed solution is then inserted into Equation (26) and a Taylor expansion around $\mathbf{x}_{\mathrm{eq}}$ is performed, yielding

$$(\dot{\mathbf{x}}_{\mathrm{eq}}(t) + \dot{\mathbf{s}}(t)) = \mathbf{A}(\mathbf{x}_{\mathrm{eq}}(t) + \mathbf{s}(t)) + \mathbf{f}(\mathbf{x}_{\mathrm{eq}}(t), t) + \left.\frac{\partial \mathbf{f}}{\partial \mathbf{x}}\right|_{\mathbf{x}=\mathbf{x}_{\mathrm{eq}}(t)} \mathbf{s}(t) + \mathbf{f}_{\mathrm{ext}}(t) + O(|\mathbf{s}(t)|^2). \tag{31}$$

Neglecting the terms of higher larger than one in $\mathbf{s}$, and using the fact that $\mathbf{x}_{\mathrm{eq}}$ is a solution of Equation (26), Equation (31) becomes

$$\dot{\mathbf{s}}(t) = \left(\mathbf{A} + \left.\frac{\partial \mathbf{f}}{\partial \mathbf{x}}\right|_{\mathbf{x}=\mathbf{x}_{\mathrm{eq}}(t)} \right) \mathbf{s}(t). \tag{32}$$

The solutions of this linear time-varying ODE indicate whether the perturbations $\mathbf{s}$ will decay or grow in time, and hence if the solution $\mathbf{x}_{\mathrm{eq}}$ is stable or not. To answer this question, Hill's method is used [16]. The perturbations are written in a specific Floquet normal form, i.e., the perturbations are decomposed as an exponential term modulated by a time-periodic function as

$$\mathbf{s}(t) = e^{\lambda t} \left(\mathbf{Q}(\omega t) \otimes \mathbf{I} \right) \mathbf{u}, \tag{33}$$

where λ is an exponential growth or decay rate, and $\mathbf{u}$ gathers the Fourier coefficients of the time-periodic function. Similarly to [16], this ansatz can be inserted into Equation (32), and using a Galerkin procedure leads to the eigenvalue problem

$$\left(\mathbf{I} \otimes \mathbf{A} - \nabla(\omega) \otimes \mathbf{I} + \frac{\partial \mathbf{b}}{\partial \mathbf{z}} \right) \mathbf{u} = \lambda \mathbf{u}, \tag{34}$$

where the Jacobian matrix on the left-hand side is most of the time obtained as a byproduct of the continuation method. Among the N_{z} eigenvalues λ (also called Hill coefficients), only N_{x} are meaningful Floquet exponents. There exists various criteria to select the relevant N_{x} eigenvalues. In this work, the N_{x} ones with smallest imaginary part modulus are selected, as in [16]. Finally, the stability of the solution $\mathbf{x}_{\mathrm{eq}}$ is concluded from the selected Floquet exponents: as per Equation (33), the solution is stable if none of them has a positive real part; it is unstable otherwise.

7 Illustration with a Duffing oscillator

A Duffing oscillator, whose response x under an external excitation f is governed by the following second-order nonlinear ODE

$$m\ddot{x}(t) + c\dot{x}(t) + kx(t) + k_3 x^3(t) = f(t), \tag{35}$$

is considered for illustration. m, c, and k are the linear mass, damping and stiffness coefficients of the oscillator, respectively, whereas k_3 is the cubic stiffness coefficient. Using the dimensionless variables $\bar{t} = t\sqrt{k/m}$ and $\bar{x} = x\sqrt{k_3/k}$, Equation (35) can be put in the dimensionless form

$$\bar{x}''(\bar{t}) + 2\zeta \bar{x}'(\bar{t}) + \bar{x}(\bar{t}) + \bar{x}^3(\bar{t}) = \bar{f}(\bar{t}), \tag{36}$$

where $\zeta = 2c/\sqrt{km}$ is the damping ratio of the oscillator, $\bar{f} = f\sqrt{k_3/k^3}$ is a dimensionless forcing, and a prime denotes a derivation with respect to the dimensionless time $\bar{t}$. When modelling control-based methods, the filter coefficients can be normalized in the same way as x (i.e., $\bar{\mathbf{w}} = \mathbf{w}\sqrt{k_3/k}$). For PLL, the frequency can be normalized consistently with the dimensionless time as $\bar{\omega} = \omega\sqrt{m/k}$, whereas the instantaneous phase θ_{pi} is already dimensionless. In the sequel, the value $\zeta = 0.05$ is selected, and the overbars are dropped to alleviate the notations, being understood that one works with a dimensionless system.

For both CBC and PLL, the developed HB models shall be verified against time simulations of the controlled Duffing oscillator modelled in Matlab/Simulink. The effect of the gains on stability will the be studied, and compared to the theoretical developments in [6, 10]. Finally, the effect of the filter dynamics on the obtained response and its stability will be investigated.

The following results have been obtained using the HB method with $N_h = 9$ harmonics and a classical alternating time-frequency procedure to evaluate the nonlinear and time-varying forces with 64 sample points.

7.1 Control-based continuation

To start with, the model of a Duffing oscillator with CBC is analyzed.

7.1.1 Verification against time simulations

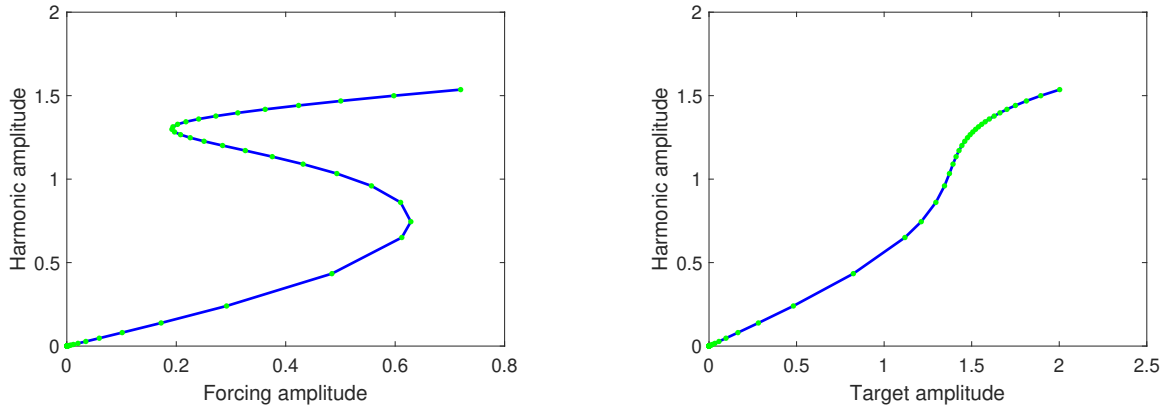

(a) (b)

Figure 4: S-curve of the Duffing oscillator at $\omega = 1.5$ obtained with the CBC method with $k_\mathrm{p} = 0$ and $k_\mathrm{d} = 0.5$: forcing amplitude f vs. harmonic amplitude (a) and target amplitude a_* vs. harmonic amplitude (b). —: HB solution, •: closed-loop stable time-simulated solution.

According to the method of Barton et al. [4], the response of a Duffing oscillator can be investigated with so-called S-curves, representing the amplitude of the response at constant excitation frequency with the abscissa representing the forcing amplitude. Figure 4a represents such a curve for $\omega = 1.5$, $k_\mathrm{p} = 0$ and $k_\mathrm{d} = 0.5$, when no filter is used (which would correspond to the converged solutions of the method in [4]). Thanks to the controller action, the part of the curve that would normally be unstable (that corresponds to the intermediate-amplitude branch in the multistable region) is stabilized, so that a full S-curve can be measured experimentally. For the time simulations, initial conditions corresponding to each point of the S-curve computed with the HB method were used, and the system was simulated for 500 periods. Time-simulated and HB results agree perfectly, verifying the developed models.

The case with $k_\mathrm{d} = 0.5$ leads to a fully stabilized S-curve because there is no folding in the drive parameter a_*, as explained in [10], and this is confirmed in Figure 4b. By contrast, a gain $k_\mathrm{d} = 0.2$ is not expected to fully stabilize the S-curve (the theoretical stability limit in [10] being $k_{\mathrm{d,crit}} = 0.3811$ in the case considered herein). Figure 5a confirms this with both HB and time-simulated[1] results. One can also observe that Hill's method very accurately predicts where instabilities set in, as time solutions initiated on the unstable branch eventually diverge from it. Finally, we note from Figure 5b that unstable solutions jump to branches nearby stable branches of the S-curve (but they are not exactly the same because the control for solutions initiated on unstable points is invasive).

[1] We note that the forcing amplitude in Figure 5a is taken equal to that of HB for readability, even though the control is invasive for unstable solutions and thus the (multi-harmonic) forcing amplitude in time simulations changes once the system settles to another branch.

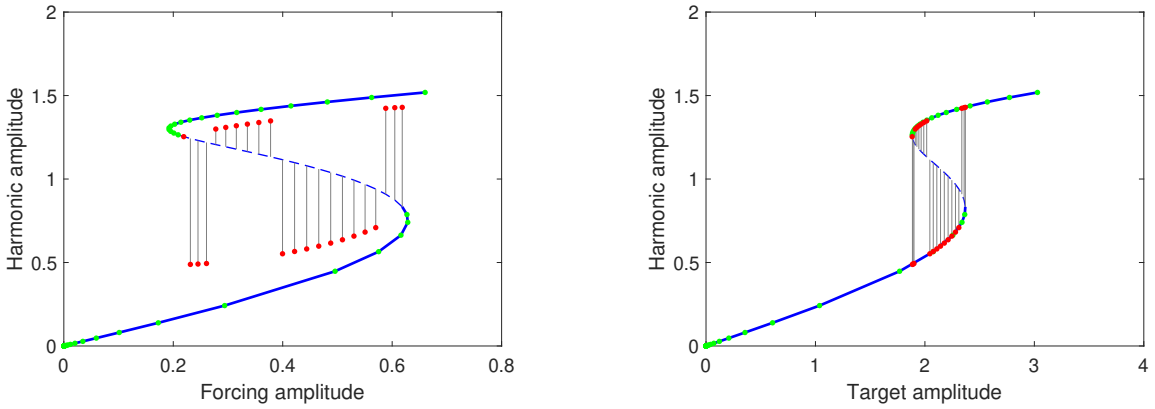

(a) (b)

Figure 5: S-curve of the Duffing oscillator at $\omega = 1.5$ obtained with the CBC method with $k_\mathrm{p} = 0$ and $k_\mathrm{d} = 0.2$: forcing amplitude f vs. harmonic amplitude (a) and target amplitude a_* vs. harmonic amplitude (b). ▬: HB solution (thick: closed-loop stable, dashed: closed-loop unstable), ●: closed-loop stable time-simulated solution, ●: closed-loop unstable time-simulated solution.

7.1.2 Controller gains and stability

Having verified the HB model against time simulations, the effect of the proportional and derivative gains on stability can now be studied. It is also possible to find the stability boundary and compare it to the theoretical results in [10] based on a one-term HB method.

Several continuation runs are performed to compute the S-curve at $\omega = 1.5$ for various values of k_p and k_d. The Floquet exponents are computed for each point of the curve, and the maximum real part of these exponents is stored. A positive maximum real part means that a part of the S-curve is unstable, indicating that the CBC fails to fully stabilize the S-curve with the selected gains.

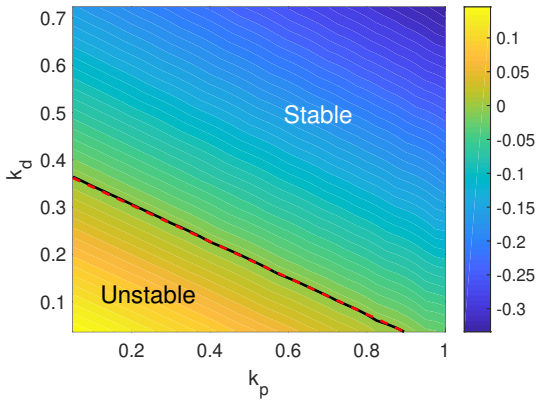

Figure 6: Maximum real part of the Floquet exponents along the S-curve for $\omega = 1.5$ and $f \in [0, 0.65]$ as a function of k_p and k_d. ▬: numerical stability boundary, ▬: theoretical stability boundary [10].

Figure 6 represents a contour plot of the maximum real part of the Floquet exponents, and highlights the stability limit (where the maximum real part equates zero). This boundary is in almost perfect agreement with its theoretical counterpart [10], further confirming the accuracy of the latter. In this simple example, stability can be achieved if large enough proportional and derivative gains are selected.

7.1.3 Effect of the filter dynamics

Abeloos et al. [14] proposed to use adaptive filters to simplify and speed up the determination of the reference signal x_*. The effect that such a filter can have on stability is now studied, considering $h = 5$ harmonics for the online Fourier decomposition.

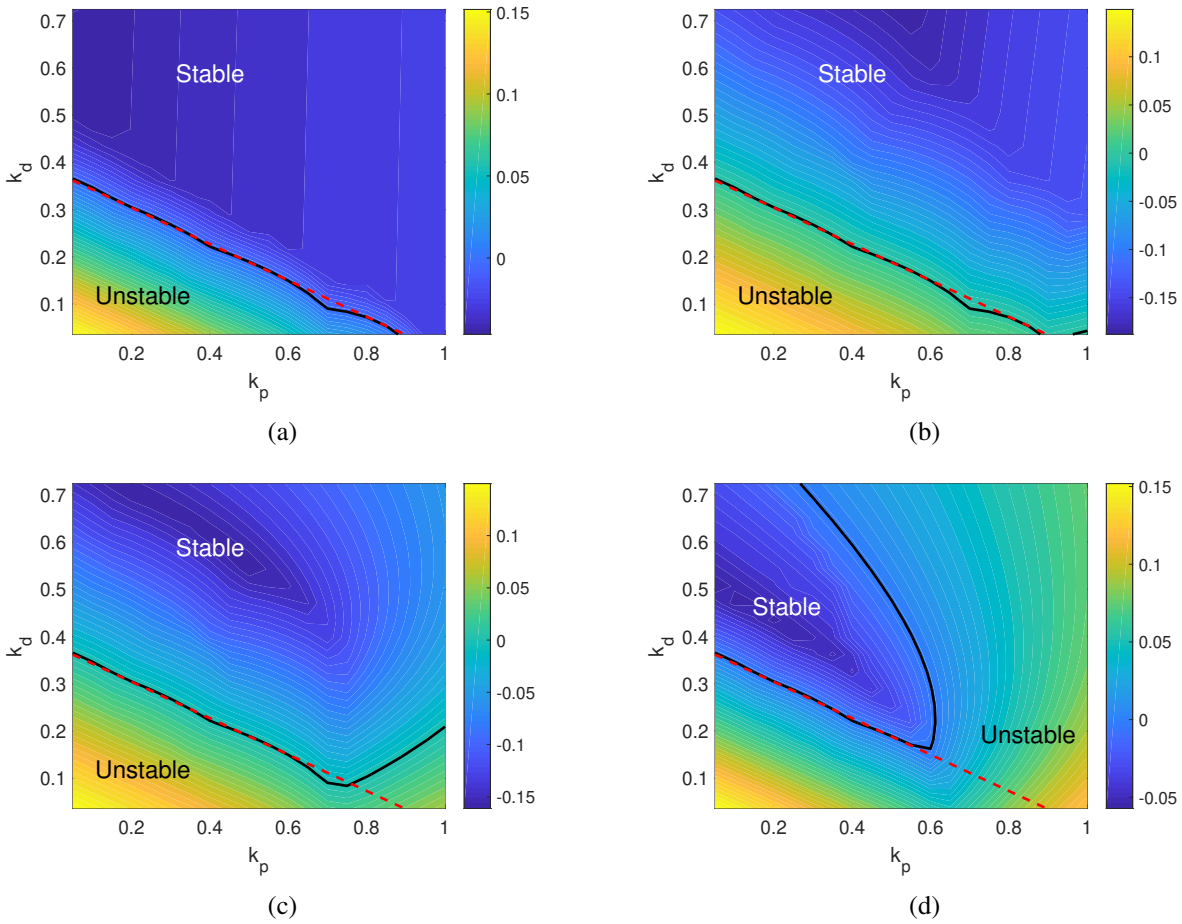

Figure 7: Maximum real part of the Floquet exponents along the S-curve for $\omega = 1.5$ and $f \in [0, 0.65]$ as a function of k_p and k_d for $\mu = 0.1$ (a), $\mu = 0.5$ (b), $\mu = 1$ (c) and $\mu = 2$ (d). ━: numerical stability boundary, ━: theoretical stability boundary [10].

Repeating the procedure followed to obtain Figure 6 for different values of the filter gain μ, the results displayed in Figure 7 are obtained. A direct comparison of the numerical values for the maximum real part of the Floquet exponents may not be straightforward, given that the system considered herein contains additional dynamics. Nevertheless, the stability boundary still marks an important qualitative change that can be compared to the case without filter. This is why the theoretical boundary limit of [10] is also plotted in Figure 7 for reference, even though it does not strictly correspond to the case studied herein.

Figures 7a and 7b show that for a low value of the filter gain, the stability boundary is very similar to the case without filter. A low value for μ corresponds to a rather slow filter. The observed results thus make sense, since the limiting case $\mu = 0$ theoretically corresponds to a case with a fixed reference x_*, i.e., the case studied in Figure 6. A high value of μ is desirable to speed up the experiment. However, as revealed by Figures 7c and 7d, this can have detrimental effects on stability. This is particularly well illustrated in Figure 7d, where large gains may lead to an unstable system, unlike the case without filter (cf. Figure 6).

7.2 Phase-locked loop

Models of a Duffing oscillator with PLL control are now considered.

7.2.1 Verification against time simulations

Similarly to Section 7.1.1, the results of the HB model are compared against time simulations over 500 periods of a PLL model built in Matlab/Simulink. However, the curve considered for verification is the NFR, and the effect of the filter cannot be neglected, because a time simulation without it is not possible. In this case, synchronous demodulation is considered, with a low-pass filter with cut-off frequency $\omega_{\mathrm{lp}} = 0.1$.

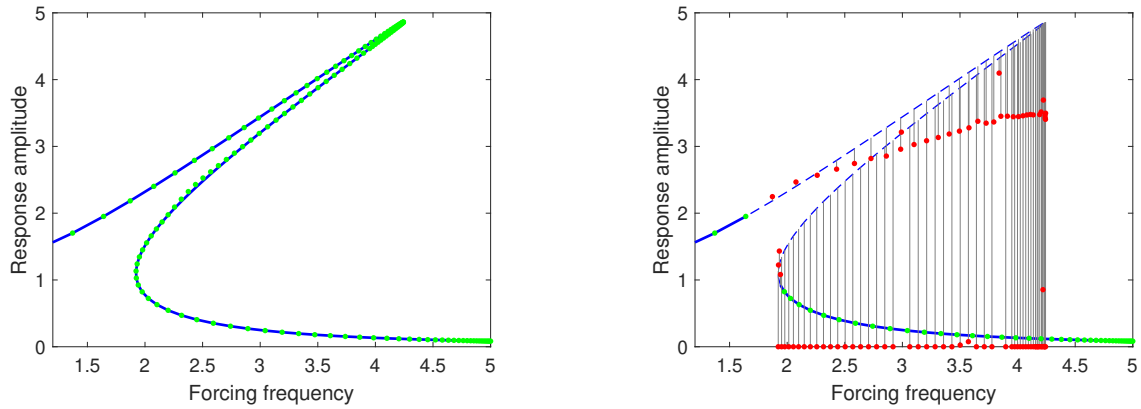

(a) (b)

Figure 8: NFR of the Duffing oscillator at $f = 2$ obtained with the PLL method with synchronous demodulation ($\omega_{\mathrm{lp}} = 0.1$): $(k_{\mathrm{p}}, k_{\mathrm{i}}) = (5, 0.5)$ (a) and $(k_{\mathrm{p}}, k_{\mathrm{i}}) = (5, 1)$ (b). —: HB solution (thick: closed-loop stable, dashed: closed-loop unstable), •: closed-loop stable time-simulated solution, •: closed-loop unstable time-simulated solution.

Figure 8 presents two cases at $f = 2$: one where the NFR is fully stabilized ($k_{\mathrm{p}} = 5$, $k_{\mathrm{i}} = 0.5$) and one where the PLL rather has a destabilizing effect compared to an open-loop case ($k_{\mathrm{p}} = 5$, $k_{\mathrm{i}} = 1$)[2]. Once again, the HB models are able to correctly represent the steady-state response of the system for stable equilibria. The limits of stable responses is also accurately predicted. In Figure 8b, time-simulated results initiated on the lower unstable branch generally have a diverging frequency that tends to infinity (hence the response amplitude tends to zero), whereas results initiated on the upper unstable branch generally feature large fluctuations of the excitation frequency.

7.2.2 Controller gains and stability

Neglecting first the filter dynamics, Figure 9 studies the effect of the controller gains on stability. In a similar fashion as the CBC, large gains appear to stabilize the system in this ideal case. Theoretical models were also established for a Duffing oscillator with a PLL [6, 9] but are based on a perturbation method requiring the damping, nonlinearity and external forcing to be small. Since these assumptions are not respected in the case considered herein, their results showed that the NFR could not be stabilized whatever the gains, and were thus inaccurate.

The stability region in Figure 9 encompasses an unstable time-simulated result (Figure 8b). Since only the filter and synchronous demodulation dynamics have been neglected, the instability must come from them. This is confirmed next.

[2]Similarly to the case of Figure 5a, the plotted frequency of the unstable time-simulated solutions is the one of the HB solution for readability.

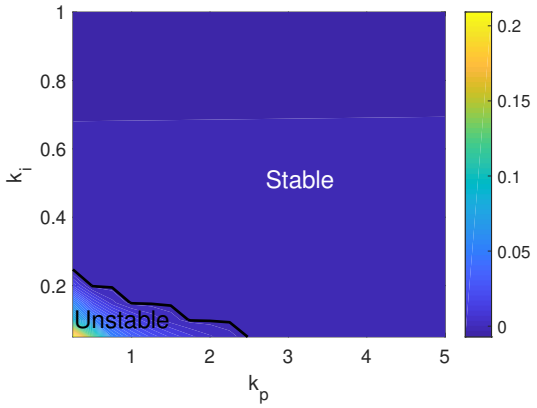

Figure 9: Maximum real part of the Floquet exponents along the NFR for $f = 2$ and $\omega \in [1.2, 5]$ as a function of k_p and k_i. ▬: numerical stability boundary.

7.2.3 Effect of the filter dynamics

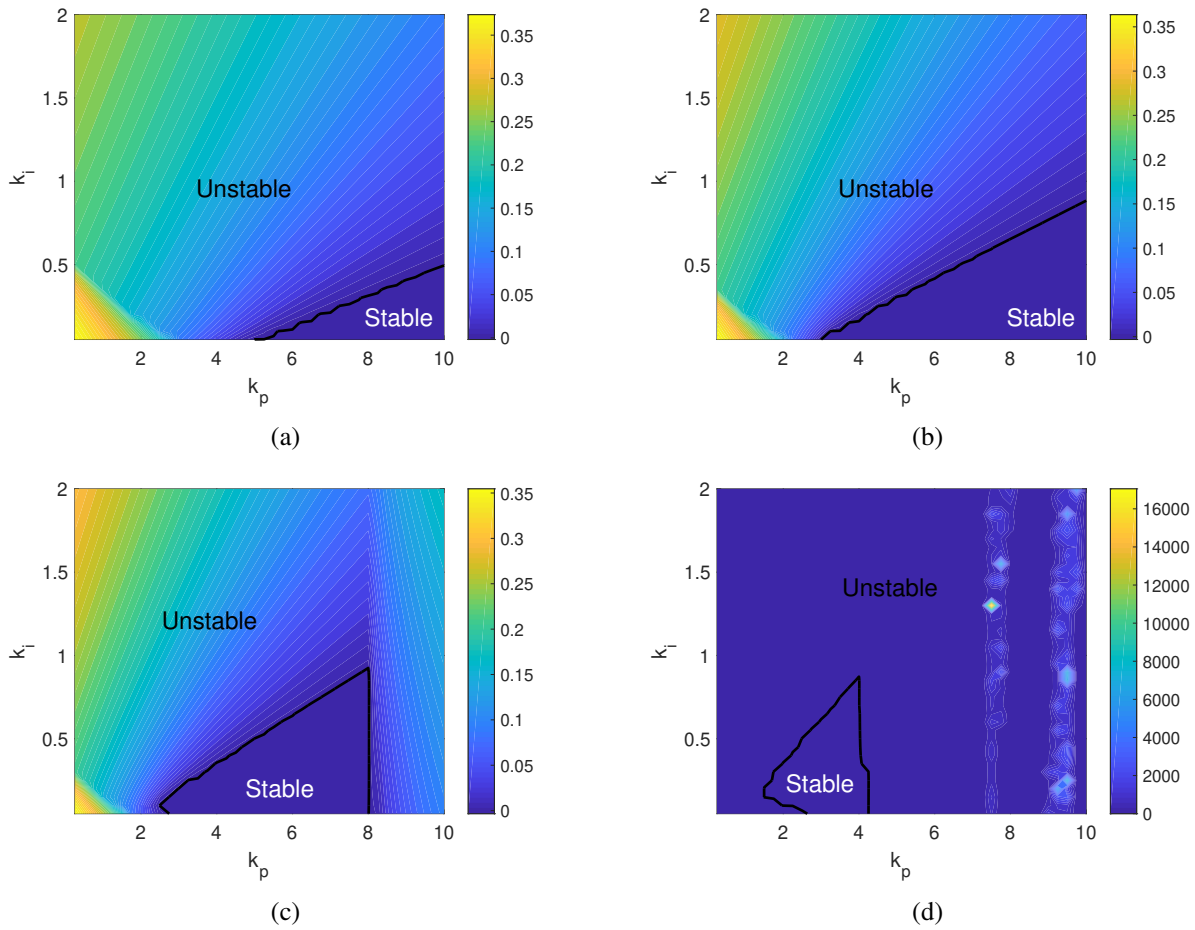

Figure 10: Maximum real part of the Floquet exponents along the NFR for $f = 2$ and $\omega \in [1.2, 5]$ as a function of k_p and k_i for $\omega_\mathrm{lp} = 0.05$ (a), $\omega_\mathrm{lp} = 0.075$ (b), $\omega_\mathrm{lp} = 0.1$ (c) and $\omega_\mathrm{lp} = 0.2$ (d). ▬: numerical stability boundary.

The effect of a low-pass filter on stability is finally assessed. Theoretical analyses in [6, 9] essentially show that a fast filter (i.e., a large ω_lp) is desirable from a stability perspective. Figure 10 shows that there is more

nuance to be brought to the discussion. On the one hand, it can be seen from Figures 10a and 10b that the left boundary of the stable region (characterized by oblique lines) indeed tends to grow the stable region as ω_{lp} increases. These oblique lines correspond to the appearance of an unstable part of the NFR on the intermediate-amplitude branch of the multistable region (corresponding to the open-loop unstable branch). On the other hand, Figures 10c and 10d show that a right boundary (a vertical line) appears for the stable region when ω_{lp} becomes large. This instability occurs on the low-frequency part of the NFR, and is due to the prominence of a second harmonic in the force. This second harmonic comes from the synchronous demodulation and was overlooked in [6, 9], but is not strongly attenuated by the low-pass filter when ω_{lp} is large and can be the cause of instabilities.

The large difference between Figures 9 and 10 stresses the importance of correctly accounting for filter dynamics in the stability analysis.

8 Conclusion

With the growing popularity of control-based methods, effective approaches for tuning their control parameters become necessary. This work developed models for such methods, and proposed to find their periodic solutions with a HB formalism together with a stability analysis. The HB models were shown to accurately represent the periodic orbits of a controlled Duffing oscillator when compared to time simulations. Furthermore, Hill's method was shown to correlate well with time-simulated results. This allowed us to investigate the effect of the control parameters on the global stability of a primary resonance. In addition, the influence of filter dynamics was assessed.

Several paths could be followed in future works. More complex structures could be considered, and the influence of non-resonant modes on stability could then be accounted for. In addition, a bifurcation tracking-based method (cf. [16]) could be used to guide the parameters tuning based on the stability boundaries.

Acknowledgements

Ghislain Raze is a Postdoctoral Researcher of the Fonds de la Recherche Scientifique - FNRS which is gratefully acknowledged.

References

[1] D. J. Ewins, *Modal Testing: Theory, Practice and Application*. John Wiley & Sons, 2009.

[2] G. Kerschen, K. Worden, A. F. Vakakis, and J.-C. Golinval, "Past, present and future of nonlinear system identification in structural dynamics," *Mechanical Systems and Signal Processing*, vol. 20, no. 3, pp. 505–592, apr 2006. [Online]. Available: https://linkinghub.elsevier.com/retrieve/pii/S0888327005000828

[3] J. Sieber and B. Krauskopf, "Control based bifurcation analysis for experiments," *Nonlinear Dynamics*, vol. 51, no. 3, pp. 365–377, feb 2008. [Online]. Available: http://link.springer.com/10.1007/s11071-007-9217-2

[4] D. A. W. Barton and J. Sieber, "Systematic experimental exploration of bifurcations with noninvasive control," *Physical Review E*, vol. 87, no. 5, p. 052916, may 2013. [Online]. Available: https://link.aps.org/doi/10.1103/PhysRevE.87.052916

[5] S. Peter and R. I. Leine, "Excitation power quantities in phase resonance testing of nonlinear systems with phase-locked-loop excitation," *Mechanical Systems and Signal Processing*, vol. 96, pp. 139–158, nov 2017. [Online]. Available: https://linkinghub.elsevier.com/retrieve/pii/S0888327017302005

[6] V. Denis, M. Jossic, C. Giraud-Audine, B. Chomette, A. Renault, and O. Thomas, "Identification of nonlinear modes using phase-locked-loop experimental continuation and normal form," *Mechanical Systems and Signal Processing*, vol. 106, pp. 430–452, jun 2018. [Online]. Available: https://linkinghub.elsevier.com/retrieve/pii/S0888327018300220

[7] T. Karaağaçlı and H. N. Özgüven, "Experimental Identification of Backbone Curves of Strongly Nonlinear Systems by Using Response-Controlled Stepped-Sine Testing (RCT)," *Vibration*, vol. 3, no. 3, pp. 266–280, sep 2020. [Online]. Available: https://www.mdpi.com/2571-631X/3/3/19

[8] E. Bureau, F. Schilder, I. Ferreira Santos, J. Juel Thomsen, and J. Starke, "Experimental bifurcation analysis of an impact oscillator—Tuning a non-invasive control scheme," *Journal of Sound and Vibration*, vol. 332, no. 22, pp. 5883–5897, oct 2013. [Online]. Available: https://linkinghub.elsevier.com/retrieve/pii/S0022460X13005142

[9] G. Abeloos, "Control-based methods for the identification of nonlinear structures," Ph.D. dissertation, University of Liège, 2022. [Online]. Available: https://hdl.handle.net/2268/295414

[10] S. Tatzko, G. Kleyman, and J. Wallaschek, "Continuation methods for lab experiments of nonlinear vibrations," *GAMM-Mitteilungen*, vol. 46, no. 2, pp. 1–13, jun 2023. [Online]. Available: https://onlinelibrary.wiley.com/doi/10.1002/gamm.202300009

[11] Y. Li and H. Dankowicz, "Model-free continuation of periodic orbits in certain nonlinear systems using continuous-time adaptive control," *Nonlinear Dynamics*, vol. 111, no. 6, pp. 4945–4957, mar 2023. [Online]. Available: https://link.springer.com/10.1007/s11071-022-08059-1

[12] H. Rezaee and L. Renson, "Noninvasive Adaptive Control of a Class of Nonlinear Systems With Unknown Parameters," pp. 1–21, jul 2023. [Online]. Available: http://arxiv.org/abs/2307.09806

[13] B. Widrow, J. Glover, J. McCool, J. Kaunitz, C. Williams, R. Hearn, J. Zeidler, J. Eugene Dong, and R. Goodlin, "Adaptive noise cancelling: Principles and applications," *Proc. IEEE*, vol. 63, no. 12, pp. 1692–1716, 1975. [Online]. Available: https://ieeexplore.ieee.org/document/1451965

[14] G. Abeloos, L. Renson, C. Collette, and G. Kerschen, "Stepped and swept control-based continuation using adaptive filtering," *Nonlinear Dyn.*, vol. 104, no. 4, pp. 3793–3808, jun 2021. [Online]. Available: https://link.springer.com/10.1007/s11071-021-06506-z

[15] A. Carusone and D. Johns, "Analogue adaptive filters: past and present," *IEE Proc. - Circuits, Devices Syst.*, vol. 147, no. 1, p. 82, 2000. [Online]. Available: https://digital-library.theiet.org/content/journals/10.1049/ip-cds_20000052

[16] T. Detroux, L. Renson, L. Masset, and G. Kerschen, "The harmonic balance method for bifurcation analysis of large-scale nonlinear mechanical systems," *Computer Methods in Applied Mechanics and Engineering*, vol. 296, pp. 18–38, nov 2015. [Online]. Available: https://linkinghub.elsevier.com/retrieve/pii/S0045782515002297